

# Cell-cell and Cell-noise Interactions of Bacterial Cells in a Shallow Circular Pool and Transitions of Collective Motions

Ryojiro Honda, Sora Umeda, and Jun-ichi Wakita

*Department of Physics, Chuo University.  
Bunkyo, Tokyo 112-8551, Japan*

We have experimentally investigated the transitions of collective motions of bacterial cells in a shallow circular pool using the bacterial species *Bacillus subtilis*. In our previous paper, we reported that the collective motions were classified into the six phases on a phase diagram with the two parameters, the reduced cell length  $\lambda$  and the cell density  $\rho$ . In the present study, we focused on the sharp transitions at  $\lambda \cong 0.1 (\equiv \lambda_{C1})$  with low values of  $\rho$  between the *random motion* phase and the *one-way rotational motion* phase. By introducing the order parameter  $Q$  which measures the aligned cell motion along the circumferential direction of a pool, the transitions at  $\lambda = \lambda_{C1}$  were clearly characterized. Based on the detailed observations of single-cell trajectories in a pool, we verified that the effect of cell-noise interactions was widely distributed. We conclude that, even in such random environment, sharp transitions of collective motions were caused by the cell-cell interactions at  $\lambda = \lambda_{C1}$ .

# 1 Introduction

Various types of ordered behavior including construction of vortex-like structures were observed in flocks of birds, schools of fish, marches of social insects, and migrations of bacteria<sup>1-9</sup>). It was also reported that the elongating bacteria produced complicated structures in folding and filling processes on an agar surface by cell multiplications<sup>10,11</sup>).

Migrating bacteria in a growing colony show a variety of collective behavior depending on environmental conditions, although bacterial colony is one of the simplest biological systems<sup>12-15</sup>). Vicsek *et al.* proposed a statistical mechanics model called the *self-propelled particle* (SPP) model to demonstrate such collective motions<sup>16-20</sup>). Their model shows the dynamical phase transition such that the ordered motions with aligned directions suddenly emerge from chaotic motions in the self-propelled particle system at a critical noise amplitude or at a critical particle density. The origin of the transition is considered to be the competition between the effect that each particle tends to be aligned in the averaged direction of its neighboring particles and the individual fluctuation of moving directions due to noise effect. The hydrodynamic motions of cells including creation and annihilation of vortices have been also universally observed in growing colonies of several bacterial species<sup>6,7</sup>). Wioland *et al.* reported that cells in a highly concentrated bacterial droplet formed a single stable vortex which can rotate both clockwise and counterclockwise directions in the droplet<sup>21</sup>). By comparing their experimental results with a model, they argued that the global confinement condition and the curvature of droplet boundaries play important roles in realizing such a steady state having a single vortex in the system. Similar self-organized structures involving vortices and clusters have been reported also in other confinement systems<sup>22-27</sup>). In experimental study, however, it is generally difficult to verify which is the essential for emergence of collective motions among cell-cell interactions, cell-boundary interactions, and individual fluctuations due to noises.

In our previous study, we experimentally investigated collective motions of bacterial cells in a shallow circular pool using bacterial species *Bacillus (B.) subtilis*<sup>28</sup>). The pools were made on the surface of an agar plate, in which collective motions of rod-shaped bacterial cells were observed. We introduced two relevant parameters, the reduced cell length  $\lambda$ , which was defined as the ratio of averaged cell length to a pool diameter, and the average cell density  $\rho$ . As shown by the phase diagram (Fig. 1), the observed collective motions have been classified into the six dynamical phases; the phases of the *random motion* (Fig. 2(a)), the *turbulent motion* (Fig. 2(b)), the *one-way rotational motion* (Fig. 2(c)), the *two-way rotational motion* (Fig. 2(d)), the *random oscillatory motion* (Fig. 2(e)) and the *ordered oscillatory motion* (Fig. 2(f)). In the *random motion* phase, bacterial cells move independently and randomly in a pool. In the *turbulent motion* phase, bacterial cells make groups showing hydrodynamic motions with creation and annihilation of vortices. In the *one-way rotational motion* phase, bacterial cells move counterclockwise along the brim of a pool keeping their axes in parallel with the brim. It suggests that the brim of a pool acts as a nearly slip boundary for a bacterial cell. Remark that in Ref. 21, however the interface of a droplet acts as a nearly no-slip boundary. In the *two-way rotational motion* phase, bacterial cells move counterclockwise in the outer region of a pool and clockwise in the inner region of a pool. In the *random oscillatory motion* phase, bacterial cells move forward and backward repeatedly in their axial directions. In this phase, the axial oscillatory motions of bacterial cells seem to be individually random and uncorrelated. In the *ordered oscillatory motion* phase, on the other hand, if we observe the system for a sufficiently long time-period, intermittent ordering of the axial directions of bacterial cells is observed. As indicated in Fig. 1 by two dashed lines perpendicular to the  $\lambda$  axis, there are two critical

values of  $\lambda$ ,  $\lambda_{C1} \cong 0.1$ ,  $\lambda_{C2} \cong 0.2$ . Crossing these two lines in the phase diagram, drastic changes occur in collective motions.

In the present study, we focused on the transitions at  $\lambda = \lambda_{C1}$  in the low values of  $\rho$  between the *random motion* phase and the *one-way rotational motion* phase. The transitions at  $\lambda = \lambda_{C1}$  were characterized by introducing the order parameter  $Q$  which measures the aligned cell motion in a circumferential direction of a pool. If the reduced cell length  $\lambda$  increases with a constant cell density  $\rho$ , then more collisions between cells occur and the alignment effect of neighboring cells is enhanced. In this sense,  $\lambda$  is a parameter representing the coupling strength of cell-cell interactions.

In order to study cell-boundary interactions and individual fluctuation of bacterial motions due to cell-noise interaction, we have examined the systems in which only a single bacterial cell is moving in a pool. As a matter of course, no cell-cell interactions exist in such single cell systems. The order parameter  $\tilde{Q}$  for the *one-way rotational motion* phase, which was properly defined for the single cell systems, did not show any systematic dependence on  $\lambda$ . We found instead that  $\tilde{Q}$  approximately linearly depended on the average value  $v_{ave}$  of cell speed. We verified that  $v_{ave}$  was determined by the frequency of change of moving direction in each trajectory of a cell. Change of moving direction of a cell will be attributed to irregularities on the bottom and the brim of a shallow pool (the surface of an agar plate) which can not be controlled in our setting of experiments.

Combining the experimental results of the original systems with a lot of bacterial cells and the single cell systems, we conclude that the transitions at  $\lambda = \lambda_{C1}$  from the *random motion* phase to the *one-way rotational motion* phase were caused by the cell-cell interactions in the systems involving uncontrolled cell-noise interactions.

All through the experiment, we used the wild-type strain OG-01 of bacterial species called *B. subtilis*<sup>12)</sup>. *B. subtilis* cells are rod-shaped with peritrichous flagella and swim straightforwardly in water by bundling and rotating their flagella. When a small amount of cells are inoculated on the surface of semisolid agar plates, they form a colony by cell motility and multiplication. Growing colonies present five different patterns depending on the two environmental parameters  $C_a$  (the concentration of agar) and  $C_n$  (the concentration of nutrient)<sup>12)</sup>. In particular, when  $C_a$  is intermediate ( $7 \text{ g/L} < C_a < 8.5 \text{ g/L}$ ) and  $C_n$  is high ( $C_n > 10 \text{ g/L}$ ), the interface of a growing colony repeatedly advances (in the migration phase) and rests (in the consolidation phase), finally yields a concentric-ring pattern. The bacterial cells at the growing front of a concentric-ring pattern have been observed to repeat elongation and contraction, synchronizing with the periodic colony growth<sup>12, 29)</sup>.

Shallow circular pools are made on the surface of an agar plate by scattering glass beads on the growing front of a concentric-ring pattern and then by removing the glass beads<sup>28)</sup>. Bacterial cells trapped in a pool show a variety of collective motions. We can control  $\lambda$  by changing the timing of making pools on the growing front, since the cell length of bacteria is different at the different time in the growing front in the concentric-ring pattern formation. Thanks to the local fluctuation of the cell density at the growing front, a variety of pools with different cell densities  $\rho$  can be made.

This paper is organized as follows. In Sect. 2, we explain the experimental procedures. Experimental results are given in Sect. 3. In Sect. 4, we give a discussion on our experimental results. Sect. 5 is devoted to giving the conclusion and discussing future problems.

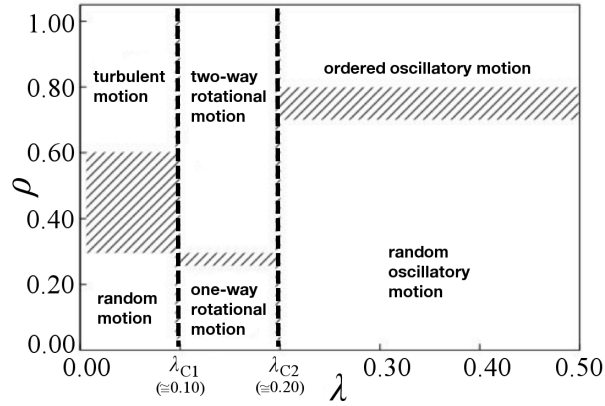


Figure 1: Phase diagram of collective motions of bacterial cells in a shallow circular pool with two parameters of  $\lambda$  and  $\rho$ . Two vertical dashed lines show the critical values  $\lambda_{C1} \cong 0.1$  and  $\lambda_{C2} \cong 0.2$ , at which the collective motions are changed drastically.

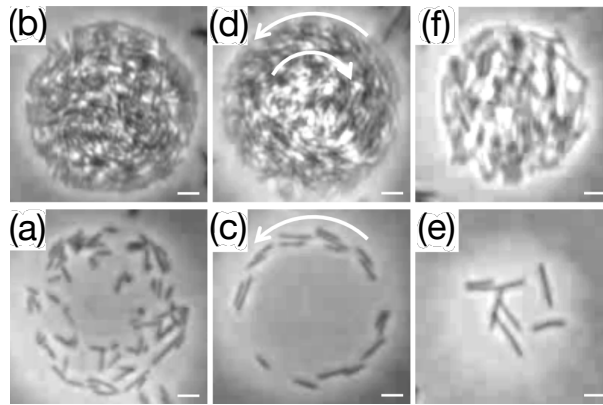


Figure 2: Snapshots of the six phases of collective motions of *B. subtilis* in a shallow circular pool. Each scale bar indicates  $10 \mu\text{m}$ . (a) the *random motion*, (b) the *turbulent motion*, (c) the *one-way rotational motion*, (d) the *two-way rotational motion*, (e) the *random oscillatory motion*, and (f) the *ordered oscillatory motion*.

## 2 Experimental Procedure

First, we prepared semisolid agar plates by following the procedures explained below. 5 g of sodium chloride (NaCl), 5 g of dipotassium hydrogen phosphate ( $\text{K}_2\text{HPO}_4$ ) and 30 g of Bacto-Peptone (Becton, Dickinson and Co.) as nutrient were dissolved in 1 L of distilled water. The environmental parameter  $C_n$  was set to 30 g/L by adjusting the concentration of Bacto-Peptone. Then, the solution was adjusted to pH 7.1 by adding 6N hydrochloric acid (HCl). Furthermore, the solution was mixed with 8.3 g of Bacto-Agar (Becton-Dickinson and Co.), which determines the softness of semisolid agar plates. The environmental parameter  $C_a$  was set to 8.3 g/L by adjusting the concentration of Bacto-Agar. The environmental condition given by these  $C_a$  and  $C_n$  values generates a typical concentric-ring pattern of *B. subtilis* colonies. The solution was autoclaved at 121°C for 15 min, and 20 ml of the solution was poured into each sterilized plastic petri dish of 88 mm inner diameter. The thickness of the semisolid agar plates was about 3.2 mm. After solidification at room temperature for 60 min, the semisolid agar plates were dried at 50°C for 90 min.

Next, we prepared bacterial suspension with an optical density of 0.5 at a wavelength of 600 nm. We inoculated 3  $\mu\text{l}$  of the bacterial suspension on the surface of each semisolid agar plate. The optical density of 0.5 corresponds to a bacterial density of about  $10^4$  cells per  $\mu\text{l}$ . The semisolid agar plates were left at room temperature for about 60 min to dry the bacterial suspension droplet.

Then, we incubated the semisolid agar plates in a humidified box at 35°C and 90% RH. Bacterial cells at the inoculation spot grew and multiplied by cell division without migration during the lag-phase period of about 7 h. After the lag-phase, the first migration started and two-dimensional colony expansion was observed. About 2 h later, they stopped migrating and entered the first consolidation phase. They did not move but underwent cell division actively for about 5 h. Afterwards, they exhibited the migration phase and the consolidation phase alternately. Thus, we obtained a concentric-ring pattern of the bacterial colonies.

After that, we scattered glass beads of  $50 \pm 2 \mu\text{m}$  diameter (Unikita, SPM-50) in the vicinity of the growing front of a concentric-ring pattern at the start of the third migration phase or the third consolidation phase of a colony growth. After we removed the beads from the agar surface using adhesive tape, circular pools were made on the surface. Bacterial cells under a bead were trapped and were moving in a pool. The pool depth was about 1  $\mu\text{m}$ , which was much smaller than the pool diameter. The thickness of each bacterial cell was about 0.5  $\mu\text{m}$ , which was approximately the same scale of the pool depth. As a result, two-dimensional motions of bacterial cells were realized in the pools. During an observation period which was set to be 10 min corresponding to the half of a cell division cycle, cell length was almost constant. We have confirmed that there were no inflow of bacterial cells into a pool and no outflow of bacterial cells from a pool. Therefore, the cell density  $\rho$  was almost constant and the collective motions of bacterial cells were stationary during an observation period. Furthermore, the water was always supplied to a pool from the agar surface, so that we were able to observe the motions of bacterial cells for relatively long time periods, which were typically more than 10 min.

We observed and video-recorded the collective motions of bacterial cells at 30 Hz with a high-speed microscope (Keyence, VW-9000) linked to an optical microscope (Nikon, DIAPHOT-TMD). We defined the area of a circular pool as the area covered by the trajectories traced by bacterial cells in the time duration 10 min. The pool diameter was calculated from the area of a pool. In the above analysis, we used an image and motion analysis library (OpenCV). On the other hand, we measured cell lengths in a snapshot captured from the video by hand. The cell density in each pool was given by dividing the

total area of bacterial cells in a pool in a snapshot by the area of a pool. To acquire the velocity field of bacterial motion in the *random motion* phase and the *one-way rotational motion* phase, we used a particle image velocimetry (PIV) software (Library, Flow-PIV).

## 3 Experimental Results

### 3.1 Transition between the random motion phase and the one-way rotational motion phase

#### 3.1.1 Introducing the order parameter

In order to clarify the differences between the cell motions in the *random motion* phase and in the *one-way rotational motion* phase, we focused on the circumferential direction component of cell velocity in a pool as explained in the following.

We performed time-series measurements at intervals of 1/30 s of the local bacterial velocity fields in the range of  $0.05 < \lambda < 0.20$ . One observation period is 60 s, so that each time-series measurement consists of 1,800 discrete velocity fields. The typical velocity fields of cell motions in the *random motion* phase and in the *one-way rotational motion* phase are shown on the snapshots in Figs. 3(a) and 3(b), respectively.

We put the origin of two-dimensional coordinates at the center of a circular pool and introduce the polar radius  $r$  and the polar angle  $\theta$ . In order to analyze the velocity fields, we consider a lattice of a square mesh of spacing 1.88  $\mu\text{m}$  on a circular pool and use the polar coordinates  $(r, \theta)$  to specify the lattice points. At each lattice point  $(r, \theta)$ ,  $\hat{\mathbf{S}}(r, \theta)$  is defined as a unit tangent vector in the circumferential direction of a pool, where the positive direction is assumed to be in the counterclockwise direction.

At each time  $t$ , the velocity vectors  $\mathbf{V}(t; r, \theta)$  were measured and their normalized vectors  $\hat{\mathbf{V}}(t; r, \theta)$  were obtained by  $\mathbf{V}(t; r, \theta)/|\mathbf{V}(t; r, \theta)|$  at all lattice points  $(r, \theta)$ . Then we defined the local order parameter  $q(t; r, \theta)$  by the following inner product

$$q(t; r, \theta) = \hat{\mathbf{V}}(t; r, \theta) \cdot \hat{\mathbf{S}}(r, \theta), \quad (1)$$

at each time  $t$  and at each lattice point  $(r, \theta)$ . Then for each  $r$ , we have averaged  $q(t; r, \theta)$  over observation time-period  $T = 60$  s (by summing over 1,800 discrete velocity fields at different times) and averaged over polar angles  $\theta \in [0, 2\pi)$ . That is, we have obtained a discretized approximation on the lattice for the quantity

$$q(r) = \frac{1}{T} \int_0^T dt \frac{1}{2\pi} \int_0^{2\pi} d\theta q(t; r, \theta). \quad (2)$$

Since the radius  $a$  of pool was distributed<sup>28)</sup>, we introduced the normalized radius coordinate as  $R = r/a$ . The  $R$ -dependent order parameter was then defined by

$$Q(R) = q(aR). \quad (3)$$

By the definition mentioned above, if all cells are in the counterclockwise *one-way rotational motion* at any place in a pool, we have  $Q(R) = 1$  for each  $R \in (0, 1)$ , while if cell motions are completely random,  $Q(R) = 0$  for each  $R \in (0, 1)$ . Hence,  $Q(R)$  will play the order parameter for the *one-way rotational motion* phase.

Figure 4(a) shows the profiles of  $Q(R)$  for  $\lambda = 0.07 < \lambda_{C1}$  and  $\lambda = 0.17 > \lambda_{C1}$ , where  $\lambda_{C1} \cong 0.1$ . The profiles have a maximum value at  $R \simeq 0.8$ , while  $Q(R) \simeq 0$  for  $R \lesssim 0.5$ . From now on, we focused on the maximum value, and define the order parameter  $Q$  of the *one-way rotational motion* phase as

$$Q = \max_R Q(R). \quad (4)$$

### 3.1.2 Behavior of order parameter $Q$

Figure 4(b) shows the  $\lambda$ -dependence of the order parameter  $Q$  in the vicinity of  $\lambda_{C1}$ . There we plotted  $Q$  only for the range of  $0.11 \leq \rho \leq 0.30$  by the following reasons. The upper limit  $\rho \simeq 0.30$  is the threshold value between the *one-way rotational motion* phase and the *two-way rotational motion* phase as shown in Fig. 1. In the *one-way rotational motion* phase, bacterial cells were often observed near the brim of a pool, so that the local cell density near the brim was effectively higher than the density  $\rho$  averaged over the whole pool. When  $\rho \geq 0.11$ , bacterial cells filled the outer region of a pool and the *one-way rotational motion* became stable. As shown in Fig. 4(b),  $Q$  has been kept at small values  $\simeq 0.3$  for  $\lambda \leq \lambda_{C1} \cong 0.1$ , while it is evident that  $Q$  increases in  $\lambda$  for  $\lambda \geq \lambda_{C1}$ . The quantity  $Q = Q(\lambda)$  indeed works as the order parameter for the *one-way rotational motion* phase. (Strictly speaking, the order parameter for the *one-way rotational motion* phase should be zero in the *random motion* phase. A possible improvement of the definition of order parameter will be proposed in Sect. 4.)



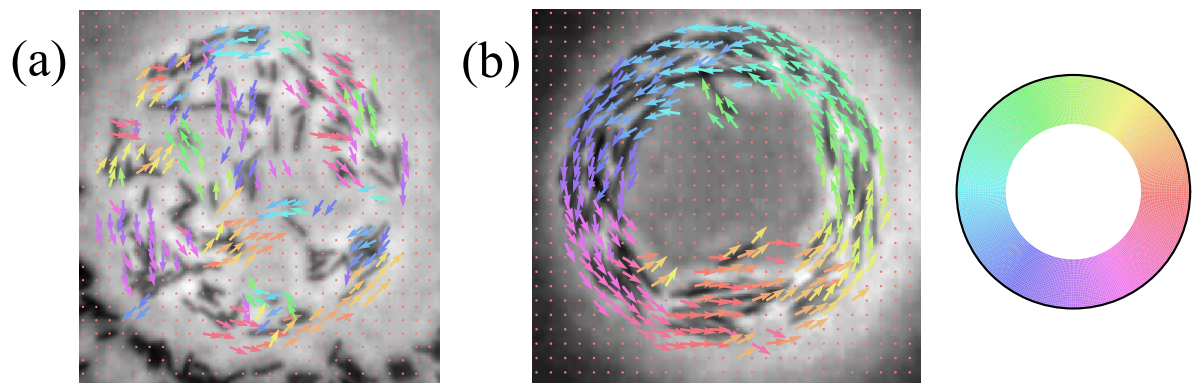


Figure 3: Typical velocity fields are shown for the *random motion* phase at  $\lambda = 0.07$  in (a) and for the *one-way rotational motion* phase at  $\lambda = 0.17$  in (b). The velocity fields are overlaid on the snapshots of bacterial cells, in which the orientations of velocity vectors are indicated by arrows with colors assigned as shown by the color ring.

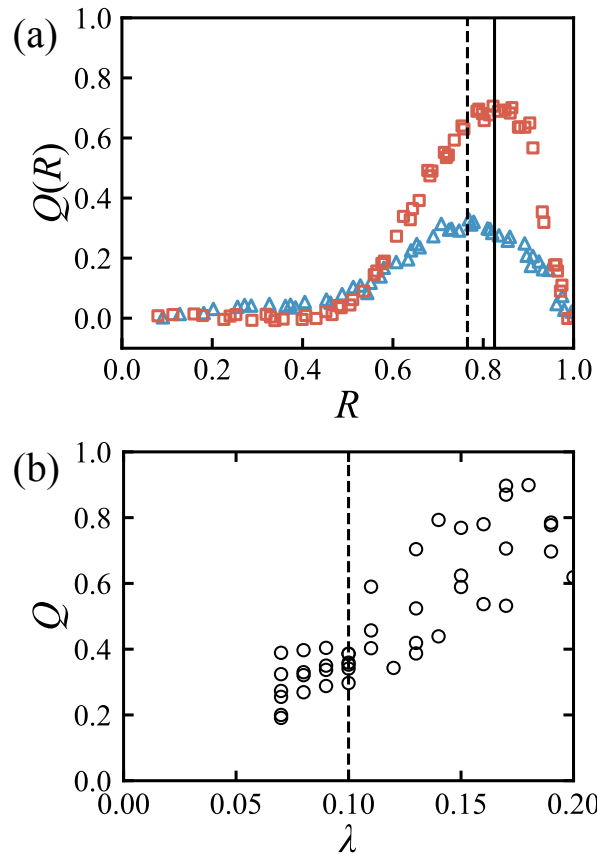


Figure 4: Measurement of the order parameter  $Q$ . (a) The profiles of  $Q(R)$  for  $\lambda = 0.07 < \lambda_{C1}$  (blue triangles) and for  $\lambda = 0.17 > \lambda_{C1}$  (red squares), where  $\lambda_{C1} \cong 0.1$ . Both profiles have maximum values around  $R \simeq 0.8$ , while have  $Q(R) \simeq 0$  for  $R \lesssim 0.5$ . (b) The values of  $Q$  are plotted against  $\lambda$  for  $0.11 \leq \rho \leq 0.30$ . For  $\lambda \leq \lambda_{C1} \cong 0.10$ ,  $Q$  has been kept at small values  $\simeq 0.3$ , while  $Q$  evidently increases in  $\lambda$  for  $\lambda \geq \lambda_{C1}$ .

## 3.2 Effects of cell-boundary interactions and cell-noise interactions

### 3.2.1 Characterization of cell motions in the single cell systems

In order to examine the effects of cell-boundary interactions and cell-noise interactions on the transitions between the *random motion* phase and the *one-way rotational motion* phase, we have examined the single cell systems such that only one bacterial cell is moving in each pool. In the original systems with a lot of bacterial cells in each pool, the cell-cell interactions will be effective. They may cause the tendency of the bacterial motions to make the individual direction of motion to be aligned with the averaged moving-direction of the neighboring cells, and also the repulsive effects between bacterial cells. As a matter of course, no cell-cell interactions exist in the single cell system.

First, we performed tracking a bacterial cell in each single cell system at intervals of 1/30 s for the time duration 600 s. Again we use the two-dimensional polar coordinate system with the origin set at the center of a pool. For each trajectory of the geometric center of a cell, we have obtain a time series of 18,000 polar coordinates  $(r(t), \theta(t))$ . Figure 5(a) shows a typical realization of trajectory for 1 s.

Then, we have evaluated the time-series velocity vectors  $\mathbf{v}(r(t), \theta(t))$  from the differences of successive polar coordinates  $(r(t), \theta(t))$ . We calculated the inner products of the normalized velocity vectors  $\hat{\mathbf{v}}(r(t), \theta(t))$  defined as  $\mathbf{v}(r(t), \theta(t))/|\mathbf{v}(r(t), \theta(t))|$  and the unit tangent vectors  $\hat{\mathbf{s}}(r(t), \theta(t))$  defined as the unit vectors in the circumferential direction of a pool at the polar coordinates  $(r(t), \theta(t))$ . The positive direction of  $\hat{\mathbf{s}}(r(t), \theta(t))$  is assumed to be in the counterclockwise direction. We checked the behavior of the time-average of the inner products defined as

$$\tilde{Q}(T) = \frac{1}{T} \sum_{t=0}^T \hat{\mathbf{v}}(r(t), \theta(t)) \cdot \hat{\mathbf{s}}(r(t), \theta(t)), \quad (5)$$

by changing the averaging time duration  $T$ . Figure 5(b) shows  $\tilde{Q}(T)$  as a function of  $T$ . This approached asymptotically to the value for  $T = 600$  s which is shown by the dotted line in Fig. 5(b). By this consideration, we defined the order parameter  $\tilde{Q}$  for the single cell systems by  $\tilde{Q}(600)$ ;  $\tilde{Q} = \tilde{Q}(600)$ .

### 3.2.2 Behavior of order parameter $\tilde{Q}$

Figure 6(a) shows the plots of the order parameter  $\tilde{Q}$  against  $\lambda$  in the range of  $0 < \lambda < 0.20$ . We note that  $\tilde{Q}$  was always positive, which implies that bacterial cells tend to move counterclockwise along the brim of a pool. This is due to the cell-boundary interactions. The values of  $\tilde{Q}$  were widely distributed between 0 and 1, and seemed to have no systematic dependence on  $\lambda$ . The critical value  $\lambda_{C1}$  found in the original collective motions become meaningless in the single cell systems.

Then, we study the average of bacterial cell speeds  $v(= |\mathbf{v}(r(t), \theta(t))|)$  over the time duration 600 s, which is denoted as  $v_{\text{ave}}$ . Figure 6(b) shows the plots of the order parameter  $\tilde{Q}$  against the time-average speed  $v_{\text{ave}}$ .  $\tilde{Q}$  seemed to increase in proportion to  $v_{\text{ave}}$ .

### 3.2.3 Distributions of cell speed $v$

In order to know what determines time-average speed  $v_{\text{ave}}$  of a bacterial cell in the single cell systems, we compared the distributions of cell speed  $v$  in time for different values of  $v_{\text{ave}}$ . Figure 7(a) shows the histograms of the cell speed  $v$  for different values of  $v_{\text{ave}}$ . Each histogram was made from 18,000 successive cell speeds  $|\mathbf{v}(r(t), \theta(t))|$ . The bin range was set from 0 to 100  $\mu\text{m/s}$  with the bin width 1  $\mu\text{m/s}$ . The total area of the histograms were normalized to be one, so that they give probability densities.

The three vertical lines indicate the values of  $v_{\text{ave}}$  of each histogram which are  $20.5 \mu\text{m/s}$  (dotted line),  $35.2 \mu\text{m/s}$  (dashed line) and  $51.1 \mu\text{m/s}$  (solid line) from the left. These values of  $v_{\text{ave}}$  are also shown by the colored circles in Fig. 6(b). The probability densities of speeds have two peaks. One of them is almost at  $v \cong 0 \mu\text{m/s}$  and another one is at larger values  $v \gtrsim 30 \mu\text{m/s}$ . The trajectories of a bacterial cell for the different values of  $v_{\text{ave}}$  in Fig. 7(a) are shown for 60 s in Fig. 7(b). Namely, the left, the middle and the right pictures in Fig. 7(b) correspond to the distributions of  $v$  for  $v_{\text{ave}} = 20.5 \mu\text{m/s}$ ,  $35.2 \mu\text{m/s}$  and  $51.1 \mu\text{m/s}$  in Fig. 7(a), respectively. The trajectories seemed to become uncomplicated as  $v_{\text{ave}}$  increased.

Here, we checked the dependence of  $v_{\text{ave}}$  on  $\lambda$ . Figure 7(c) shows that the values of  $v_{\text{ave}}$  were widely distributed between  $10 \mu\text{m/s}$  and  $60 \mu\text{m/s}$ , and did not seem to have any systematic dependence on  $\lambda$ .

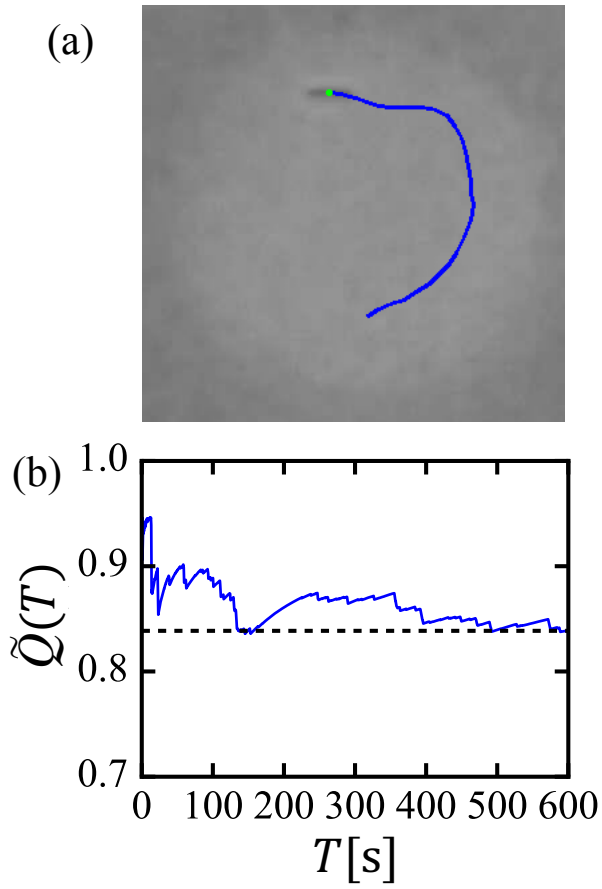


Figure 5: Tracking a bacterial cell in the single cell system. (a) Trajectory of the geometric center of a bacterial cell for 1 s. (b) Time-average of the inner products  $\tilde{Q}(T)$  defined by Eq. (5) is shown as a function of averaging time  $T$ .

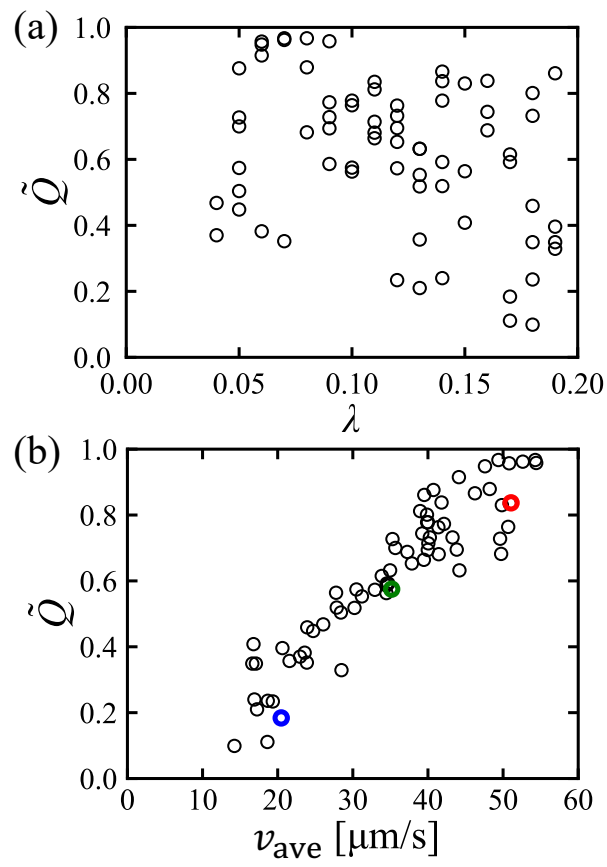


Figure 6: Behavior of the order parameter  $\tilde{Q}$  in the single cell systems. (a) The order parameters  $\tilde{Q}$  are plotted against  $\lambda$  ( $0 < \lambda < 0.2$ ). (b) The order parameters  $\tilde{Q}$  are plotted against  $v_{\text{ave}}$ .

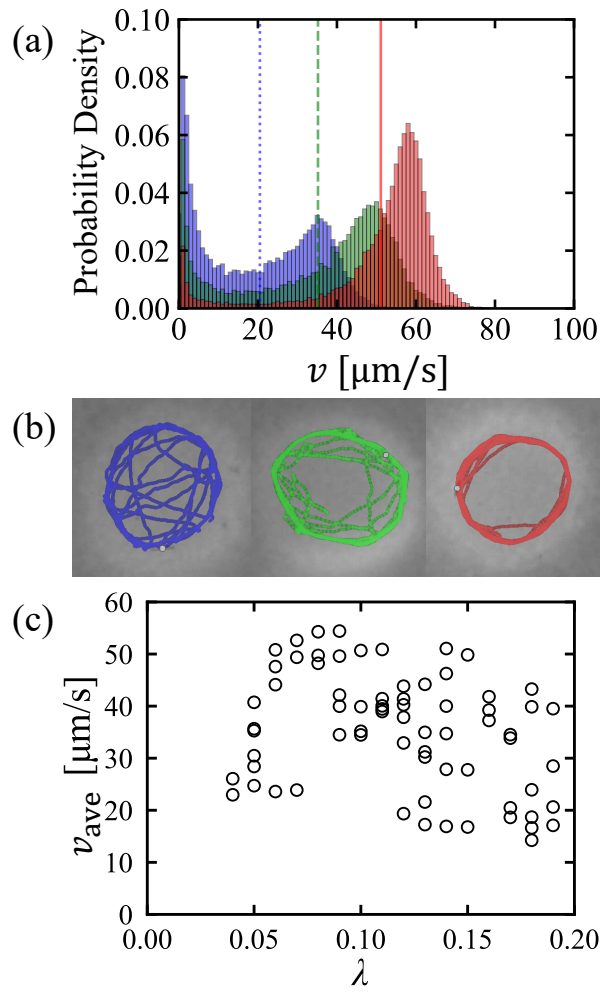


Figure 7: Comparison of the distributions of cell speed  $v$ . (a) The probability densities of cell speed  $v$  distributed in time are shown for the different values of  $v_{\text{ave}}$ , 20.5, 35.2, and 51.1  $\mu\text{m/s}$ . These values correspond to the colored circles in Fig. 6(b). (b) The trajectories of a bacterial cell for the different values of  $v_{\text{ave}}$  in (a) are shown for 60 s. The left, the middle, and the right pictures correspond to the distributions of  $v$  for  $v_{\text{ave}} = 20.5, 35.2,$  and  $51.1 \mu\text{m/s}$ , respectively. (c) The values of  $v_{\text{ave}}$  are plotted against  $\lambda$ .

## 4 Discussion

In this section, we discuss the transitions of collective motions of bacterial cells in a shallow circular pool between the *random motion* phase and the *one-way rotational motion* phase, when the reduced cell length  $\lambda$  was changed in the vicinity of  $\lambda_{C1}$ .

First we view the dependence of  $Q$  on  $\lambda$  shown in Fig. 4(b). Change of the behavior of  $Q$  was recognized at  $\lambda = \lambda_{C1}$ . From the microscopic observation for  $\lambda \geq \lambda_{C1}$  (in the *one-way rotational motion* phase), we found that the bacterial cells were localized in the outer region of a pool and were moving counterclockwise along the brim of a pool. (The outer region is defined as the range of  $0.6 \leq R \leq 1.0$  from the profile of  $Q$  in Fig. 4(a).) As shown by Fig. 4(a), the value of  $R$  at which  $Q(R)$  attained its maximum was about 0.8. Therefore the order parameter  $Q$  defined by  $\max_R Q(R)$  indicates the typical value of  $Q(R)$  for bacterial cell motions. On the other hand, from the microscopic observation, we found that also in the systems with  $\lambda \leq \lambda_{C1}$  (in the *random motion* phase) the bacterial cells in the outer region of a pool seemed to have a tendency to move counterclockwise along the brim of a pool. This tendency is thought to be due to the cell-boundary interactions. As a result, the values of  $Q$  were in the range of  $0.2 \leq Q \leq 0.4$  even for  $\lambda \leq \lambda_{C1}$  as shown in Fig. 4(a). We considered, however, the typical behavior of bacterial cell motions for  $\lambda \leq \lambda_{C1}$  should be measured in the inner region of a pool apart from the cell-boundary interactions. Then, here we redefine the order parameter  $Q$  as the value of  $Q(R)$  at  $R = 0.3$  (the middle position of the inner region). Figure 8 shows the dependence of  $Q$  on  $\lambda$ , in which the values of  $Q$  became almost zero for  $\lambda \leq \lambda_{C1}$ .

The behavior of  $Q$  reminds us the dynamical phase transition in SPP model<sup>1,16,17</sup>). In SPP model, the transition of the collective motion of self-propelled particles is caused by the competitive relation between the effect that the individual moving direction is aligned with the averaged moving direction of its neighboring particles and the fluctuation of moving direction due to noise effect. There, for a specified particle, neighboring particles are defined as the particles in a circle of some given radius (interaction radius) centered at the position of the focused particle. The transition occurs at the critical noise amplitude or at the critical particle density in SPP model. On the other hand, in our experiment the transitions were observed at the critical value of the reduced cell length  $\lambda_{C1}$ . From the microscopic observation, we saw that rod-shaped bacterial cells had the tendency to be aligned their moving directions each other. This tendency seemed to be monotonically increasing as the length of bacterial cells increased. Therefore,  $\lambda$  is considered to correspond to the interaction radius in SPP model.

Next we discuss the effect of cell-noise interactions. We have examined the single cell systems and defined the order parameter  $\tilde{Q}$  for the *one-way rotational motion* phase. Figure 6(a) shows the plots of the order parameter  $\tilde{Q}$  against  $\lambda$ . The values of  $\tilde{Q}$  were widely distributed between 0 and 1 for  $0 < \lambda < 0.2$ . No critical value  $\lambda_{C1}$  was found in the plots of  $\tilde{Q}$  in the single cell systems having no cell-cell interaction. This result indicates that the transitions between the *random motion* phase and the *one-way rotational motion* phase are caused by the cell-cell interactions.

Finally, we consider the dependence of  $\tilde{Q}$  on  $v_{ave}$ . The distributions of cell speed  $v$  for different values of  $v_{ave}$  had two peaks as shown in Figure 7(a). One of them was almost at  $v \cong 0$   $\mu\text{m/s}$  and another one was at  $v \gtrsim 30$   $\mu\text{m/s}$ . When the frequencies of the peaks at  $v \cong 0$   $\mu\text{m/s}$  were low and those at  $v \gtrsim 30$   $\mu\text{m/s}$  were high,  $v_{ave}$  became large. Therefore, we can say that  $v_{ave}$  is determined by the ratio of the frequencies at  $v \cong 0$   $\mu\text{m/s}$  to the frequencies at  $v \gtrsim 30$   $\mu\text{m/s}$ . In the microscopic observation, a moving bacterial cell was observed to stop to change its direction. Hence the frequency of the peak at  $v \cong 0$   $\mu\text{m/s}$  represents the frequency of the change of moving direction. In other words,  $v_{ave}$  is considered to



have a monotonically decreasing dependence on the frequency of the change of moving direction. Fig. 7(b) shows the trajectories of a bacterial cell for the different values of  $v_{\text{ave}}$ . There we see that, as  $v_{\text{ave}}$  increased, the trajectories became uncomplicated. When  $v_{\text{ave}} = 54.3 \mu\text{m/s}$ , the trajectory was almost circular and  $\tilde{Q}$  was 0.97. In this case the frequency of the change of moving direction was almost zero and the distribution of  $v$  had only one peak as shown in Fig. 9. Furthermore, we have observed that a bacterial cell sometimes changed its moving direction at the same positions in a pool. Some irregularities may exist on the bottom and the brim of a pool (the surface of an agar plate). Note that the pool had a depth about  $1 \mu\text{m}$ , which was the same scale with a diameter of a bacterial cell ( $\simeq 0.5 \mu\text{m}$ ). Therefore, we attributed the change of moving direction of a bacterial cell to the cell-noise interactions between each bacterial cell and irregularities on the surface of a pool. By the above considerations, the behavior of a bacterial cell in the single cell systems was suggested to be dependent on the competition between the cell-boundary interactions and the cell-noise interactions.

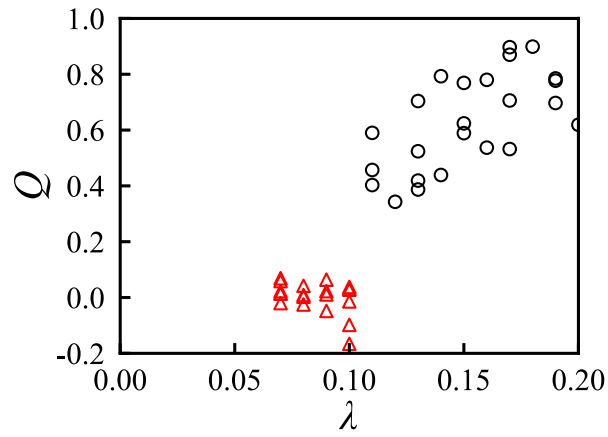


Figure 8: The dependence of the redefined order parameter  $Q$  on  $\lambda$ .

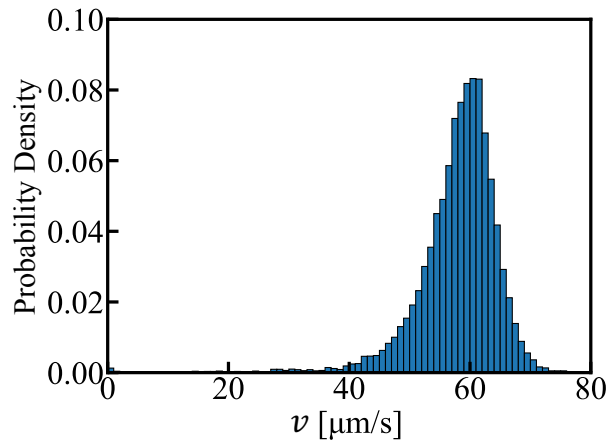


Figure 9: One peak histogram for the distribution of cell speeds  $v$  when  $v_{\text{ave}} = 54.3 \mu\text{m/s}$ .

## 5 Conclusion and Future Problems

In SPP model<sup>1,16,17</sup>), the transitions between disordered state and ordered state are caused by changing the particle density or the noise amplitude. The critical values exist for each parameter. In other words, the dynamical transitions are realized by the competitions between the effects that each particle tends to be aligned in averaged direction of its local neighborhood particles and the fluctuation of moving directions due to noise effect. While in our experiment, only by controlling  $\lambda$ , the transitions between the *random motion* phase and the *one-way rotational motion* phase occur at  $\lambda = \lambda_{C1}$ .

In our experiment, the transitions were observed in the original systems, but were not observed in the single cell systems (see Figs. 4(b) and 6(a)). Thus the transitions were considered to be induced by the effect of cell-cell interactions.

In the single cell systems, when the average-speed  $v_{ave}$  was sufficiently high, a bacterial cell had the strong tendency to move counterclockwise along the brim of a pool. This yielded a large value of the order parameter  $\tilde{Q}$ . When  $v_{ave}$  was low, on the other hand, we obtained a small value of  $\tilde{Q}$  as shown in Fig. 6(b). As shown in Fig. 7(c)  $v_{ave}$  did not depend on  $\lambda$ .

As discussed in Sect. 4, the value of  $v_{ave}$  is considered to represent the intensity of noise effect. On the other hand,  $\lambda$  represents the effective length which affects the repulsion and the alignment of bacterial cells. That is,  $\lambda$  provides the interaction range of the cell-cell interaction. Fig. 7(c) implies that these two factors were uncorrelated.

From the above considerations, we conclude the following. In the present experimental systems, we were able to control the interaction range between bacterial cells by changing  $\lambda$ , but were not able to control the noise intensity. Such a situation is well described in Fig. 4(b) and Fig. 8, which show the  $\lambda$ -dependence of the original order parameter  $Q$  defined in Sect. 3.1.1 and its modified version defined in Sect. 4. The scattering of the plots of  $Q$  in these graphs is caused by the noise effect, which were not controlled. Nevertheless, the parameter  $\lambda$  is still relevant to describe the transitions, since the critical value  $\lambda_{C1}$  seemed to be fixed at  $\cong 0.1$  so that the order parameter  $Q$  evidently increased in  $\lambda$  for  $\lambda \gtrsim 0.1$ , while the dependence of  $Q$  on  $\lambda$  was negligible for  $\lambda \lesssim 0.1$  for all systems which we examined.

In the present work, we have studied three different effects, which are caused by the cell-cell interactions, the cell-boundary interactions, and the cell-noise interactions, respectively. By properly changing the definition of the order parameter  $Q$ , we reduced the effect of cell-boundary interaction in the *random motion* phase in the description of the transitions using  $Q$ . Although the effect of cell-noise interactions was not able to be controlled in our systems, and hence the obtained values of  $Q$  were scattering, we have verified that a critical value  $\lambda_{C1}$  was well defined as the threshold at which the  $\lambda$ -dependence of  $Q$  definitely changed. We conclude that in the transitions between the *random motion* phase and the *one-way rotational motion* phase, the cell-cell interactions give the primary effect.

More detailed study of the cell-noise interactions and of the cell-boundary interactions are required in order to give more precise description of the transitions including critical phenomena. In the present paper we have reported our work on the transitions at  $\lambda = \lambda_{C1}$  with low values of  $\rho$ . The transitions at  $\lambda = \lambda_{C1}$  with higher values of  $\rho$  (between the *turbulent motion* phase and the *two-way rotational motion* phase) as well as those at  $\lambda = \lambda_{C2}$  will be important future problems. Extensions of SPP model suitable to describe the present experimental results are also required.

## Acknowledgement

The authors would like to thank Mitsugu Matsushita, Helmut R. Brand, Takuma Narizuka, Yoshihiro Yamazaki, Yusuke T. Maeda, and Hirofumi Wada for useful discussion. They also thank Makoto Katori for careful reading of the manuscript and useful comments. JW is supported by a Chuo University Grant for Special Research and by a Grant-in-Aid for Exploratory Research (No. 15K13537) from the Japan Society for the Promotion of Science (JSPS).

- 1) T. Vicsek and A. Zafeiris, *Physics Reports*, **517**, 71 (2012).
- 2) M. Ballerini, N. Cabibbo, R. Candelier, A. Cavagna, E. Cisbani, I. Giardina, V. Lecomte, A. Orlandi, G. Parisi, A. Procaccini, M. Viale, and V. Zdravkovic, *Proc. Natl. Acad. Sci. U.S.A.* **105**, 1232 (2008).
- 3) A. Cavagna, A. Cimarelli, I. Giardina, G. Parisi, R. Santagati, F. Stefanini, and M. Viale, *Proc. Natl. Acad. Sci.* **107** 11865 (2010).
- 4) C. K. Hemelrijk, H. Hildenbrandt, J. Reinders, and E. J. Stamhuis, *Ethology* **116**, 1099 (2010).
- 5) C. Becco, N. Vandewalle, J. Delcourt, and P. Poncin, *Physica A*, **367**, 487 (2006).
- 6) A. Czirók, E. Ben-Jacob, I. Cohen, and T. Vicsek, *Phys. Rev. Lett.* **54**, 1791 (1996).
- 7) J. Wakita, I. Ràfols, H. Itoh, T. Matsuyama, and M. Matsushita, *J. Phys. Soc. Jpn.* **67**, 3630 (1998).
- 8) A. Sokolov and I. S. Aranson, *Phys. Rev. Lett.* **109**, 248109 (2012).
- 9) H. H. Wensink, J. Dunkel, S. Heidenreich, K. Drescher, R. E. Goldstein, H. Löwen, and J. M. Yeomans, *Proc. Natl. Acad. Sci. U. S. A.* **109**, 14308 (2012).
- 10) R. Honda, J. Wakita, and M. Katori, *J. Phys. Soc. Jpn.* **84**, 114002 (2015).
- 11) G. Mamou, G. B. M. Mohan, A. Rouvinski, A. Rosenberg, and S. Ben-Yehuda, *Cell Reports* **14** 1850 (2016).
- 12) M. Matsushita, F. Hiramatsu, N. Kobayashi, T. Ozawa, Y. Yamazaki, and T. Matsuyama, *Biofilms* **1**, 305 (2004).
- 13) A. Nakahara, Y. Shimada, J. Wakita, M. Matsushita, and T. Matsuyama, *J. Phys. Soc. Jpn.* **65**, 2700 (1996).
- 14) F. Hiramatsu, J. Wakita, N. Kobayashi, Y. Yamazaki, M. Matsushita, and T. Matsuyama, *Microbes Environ.* **20**, 120 (2005).
- 15) R. Tokita, T. Katoh, Y. Maeda, J. Wakita, M. Sano, T. Matsuyama, and M. Matsushita, *J. Phys. Soc. Jpn* **78**, 074005 (2009).
- 16) T. Vicsek, *Fluctuations and Scaling in Biology* (Oxford University Press, New York, 2001).
- 17) T. Vicsek, A. Czirók, E. Ben-Jacob, I. Cohen, and O. Shochet, *Phys. Rev. Lett.* **75**, 1226 (1995).
- 18) A. Czirók, H. E. Stanley, and T. Vicsek, *J. Phys. A* **30**, 1375 (1997).
- 19) H. Chaté, F. Ginelli, G. Grégoire, and F. Raynaud, *Phys. Rev. E*, **77**, 046113 (2008).
- 20) G. Baglietto, E. V. Albano, and J. Candia, *Interface Focus*, **2**, 708 (2012).
- 21) H. Wioland, F. G. Woodhouse, J. Dunkel, J. O. Kessler, and R. E. Goldstein, *Phys. Rev. Lett.* **110**, 268102 (2013).
- 22) H. Wioland, F. G. Woodhouse, J. Dunkel, and R. E. Goldstein, *Nat. Phys.* **12**, 341 (2016).

- 23) K. Beppu, Z. Izri, J. Gohya, K. Eto, M. Ichikawa, and Y. T. Maeda, *Soft Matter* **13**, 5038 (2017).
- 24) D. Nishiguchi, I. S. Aranson, A. Snezhko, and A. Sokolov, *Nat. Commun.* **9**, 4486 (2018).
- 25) K. T. Wu and J. B. Hishamunda, *Science* **355**, 6331 (2017).
- 26) A. Bricard, J.-B. Caussin, D. Das, C. Savoie, V. Chikkadi, K. Shitara, O. Chepizhko, F. Peruani, D. Saintillan, and D. Bartolo, *Nat. Commun.* **6**, 7470 (2015).
- 27) A. Deblais, T. Barois, T. Guerin, P. H. Delville, R. Vaudaine, J. S. Lintuvuori, J. F. Boudet, J. C. Baret, and H. Kellay *Phys. Rev. Lett.* **120**, 188002 (2018).
- 28) J. Wakita, S. Tsukamoto, K. Yamamoto, M. Katori, and Y. Yamada, *J. Phys. Soc. Jpn.* **84**, 124001 (2015).
- 29) J. Wakita, H. Shimada, H. Itoh, T. Matsuyama, and M. Matsushita, *J. Phys. Soc. Jpn.* **70**, 911 (2001).